

Determination of Evaporation Rates and Vapor Pressures of Very Low Volatility Compounds: A Study of the C₄–C₁₀ and C₁₂ Dicarboxylic Acids

Christopher D. Cappa,^{*,†,‡} Edward R. Lovejoy,[†] and A. R. Ravishankara^{†,§}

Chemical Sciences Division, Earth System Research Laboratory, NOAA, Boulder, Colorado 80305, Cooperative Institute for Research in the Environmental Sciences, University of Colorado, Boulder, Colorado 80305, and Department of Chemistry and Biochemistry, University of Colorado, Boulder, Colorado 80305

Received: December 18, 2006; In Final Form: February 12, 2007

A method for the measurement of evaporation rates and vapor pressures of low volatility compounds was developed and applied to the homologous series of C₄–C₁₀ and C₁₂ dicarboxylic acids. Proton-transfer chemical ionization mass spectrometry was used to follow directly the temperature-dependent evaporation rates of aerosol samples collected on a cold plate that could be heated at a known rate. The vapor pressures of the deposited compounds were derived from observed evaporation rates through application of the Hertz–Knudsen equation. Temperature programmed desorption allowed for quantification of the enthalpy (ΔH_{sub}) and entropy (ΔS_{sub}) of sublimation of the diacids and is described. A strong odd–even dependence with respect to the total carbon number was observed in the derived diacid vapor pressures, consistent with previous measurements. However, the vapor pressures from this method were systematically lower than previous measurements. Though seen in the vapor pressure, no odd–even carbon chain length dependence was readily discernible in the measured values of ΔH_{sub} and ΔS_{sub} . Perhaps most importantly, these experimental results also suggest that residual solvent molecules (from the aerosol generation process) trapped in the diacid samples can have a considerable influence on the measured thermodynamic parameters and, if not properly accounted for, may give erroneous results.

Introduction

Aerosols in the atmosphere are important on global, regional, and local scales owing to their influence on climate and composition of the atmosphere,¹ and their negative health effects.² Organic compounds are a substantial fraction of the aerosol and are derived from both primary and secondary sources.³ These secondary organic sources are the result of photo-oxidation of both anthropogenic and biogenic precursor gases, primarily through the addition of functional groups to the parent compounds. Observations of organic aerosols in the atmosphere indicate that the actual amount of organic mass is significantly greater than predicted by current models,^{4–6} although this conclusion appears to be dependent upon the region considered and identity of the most abundant precursor gases.⁷

Gas-to-particle partitioning of organic compounds depends upon the physical properties of both the oxidized gaseous organic and the aerosol because of factors such as the solubility, miscibility and absorption behavior of the semi-volatile gases onto preexisting aerosol.^{8–11} If the vapor pressures of the oxidized compounds are sufficiently low, they may also nucleate to form new particles.¹² To develop predictive models of aerosol behavior in the atmosphere, it is, therefore, desirable to have accurate values of the physicochemical properties of the aerosol precursor compounds. In particular, the temperature-dependent vapor pressures (p^0) of the pure components are needed.

Various methods exist for the measurement of vapor pressures of very low-volatility compounds, including Knudsen cell effusion,^{13,14} tandem differential mobility analysis (TDMA),^{15–17} droplet evaporation via light scattering¹⁸ and temperature programmed desorption (TPD).^{19,20} Besides these experimental approaches, group-contribution computational methods (e.g., UNIFAC^{21–24} or SPARC²⁵) also allow calculation of vapor pressures of subcooled liquids, which can be converted to solid-phase vapor pressures given knowledge of the melting temperature and enthalpy of fusion.²⁶

Diacids have been identified in atmospheric aerosols with significant abundances and in a large variety of chemical environments (e.g., in urban,^{27–30} rural,^{30–32} marine,³³ and polar^{34,35} regions) and in smog chamber experiments.^{36–40} The vapor pressures of some of the homologous straight-chain dicarboxylic acids (HOOC(CH₂)_{*n*}COOH) are in reasonable agreement, but for others the results depend significantly on the experimental methods.^{13,14,16,17,20} Additionally, there is little consistency in the variation of the measured enthalpies of sublimation (ΔH_{sub}) as a function of carbon chain length (N_c). The variability of calculated diacid vapor pressures is similarly large.^{23–25,41}

To address some of the disparities in the existing experimental and computational determinations of the physical properties of the diacids, we have developed a method that utilizes temperature programmed desorption to measure vapor pressures and ΔH_{sub} values of low-volatility compounds. The method described herein shares some general similarities to the TPD experiments of Ziemann and co-workers;^{19,20} however, our method allows for direct measurement of temperature-dependent evaporation rates (and therefore vapor pressures). Proton-transfer

* Corresponding author. E-mail: christopher.cappa@noaa.gov.

† NOAA.

‡ Cooperative Institute for Research in the Environmental Sciences, University of Colorado.

§ Department of Chemistry and Biochemistry, University of Colorado.

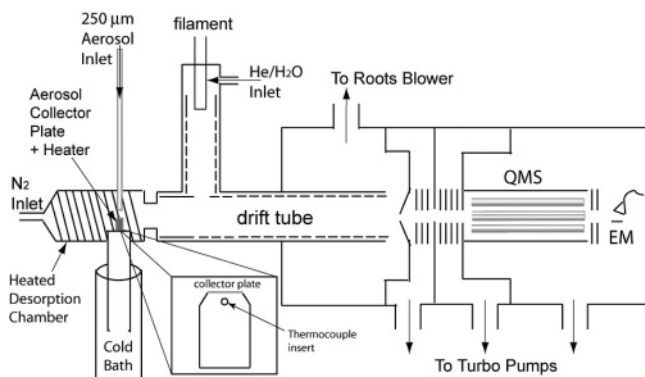


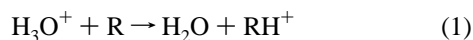
Figure 1. Schematic of the experimental apparatus.

chemical ionization mass spectrometry (PT-CIMS) was used for detection of the evaporated molecules.

In this paper, we present our results and compare our results with those from other experimental methods. Our results indicate that the vapor pressures of the homologous C_4 – C_{10} diacids are lower than previously reported values, and therefore that the partitioning of the diacids to the particle phase will be more significant than has been previously suggested.

Experimental Methods

PT-CIMS. In PT-CIMS an organic trace gas, R , is ionized via a proton-transfer reaction with H_3O^+ ions, i.e.



Both analyte and reagent ions were extracted from the ion drift tube into a quadrupole mass spectrometer for mass-specific detection. A schematic of the experimental setup is shown in Figure 1. The PT-CIMS system used in these studies has been described previously.⁴² For these studies the typical operating pressure was ~ 0.5 – 0.7 Torr with $E/N \sim 103$ – 108 Td ($1 \text{ Td} = 10^{-17} \text{ V cm}^2$). H_3O^+ was the dominant reagent ion, and $H_2O \cdot H_3O^+$ contributed $< 3\%$ to the total reagent ion signal and O_2^+ and N_2^+ contributed $< 1\%$.

H_3O^+ was generated by electron impact ionization of H_2O vapor added into $3.5 \text{ STP cm}^3 \text{ s}^{-1}$ of He ($\text{STP} = 1 \text{ atm}, 273 \text{ K}$). Nitrogen was added through the back end of the main drift tube at $5.2 \text{ STP cm}^3 \text{ s}^{-1}$ of N_2 such that the total flow rate was $8.7 \text{ STP cm}^3 \text{ s}^{-1}$.

Aerosol Production and Deposition. Polydisperse aerosols were produced by atomizing ~ 1 – 2 wt % methanol solutions of diacids. The aerosols were dried by passing them through a horizontal flow tube partially filled with a $13\times$ molecular sieve with a residence time of ~ 3 min. The aerosols were introduced into the desorption chamber through a 30 cm long, 0.25 mm i.d. capillary inlet. The inlet served to focus the aerosols into a well-defined, collimated beam. The aerosol beam was directed at the center of a circular flat-plate collector located < 1 mm from the capillary exit. The collected aerosol was visible as a small, solid, cone-shaped mound with a base diameter (d) and height (h) that ranged from ~ 0.2 to 0.6 mm; typically $d \sim h$. For each experiment an image of the sample was collected so that d and h could be determined via reference to the collector diameter (6.65 mm).

Temperature Programmed Desorption. The aerosol collector was mounted onto a cartridge heater, which was soldered onto a copper tube support. The collector, ~ 1 cm in height, was composed of a thin stainless steel plate soldered onto a brass base that was tapered to the top surface over a distance

of ~ 2 mm, from 8.85 mm to 6.65 mm diameter (see Figure 1). The collector could be cooled to temperatures as low as 250 K by immersing the copper tube into a liquid nitrogen bath or heated to > 430 K through use of the cartridge heater. The temperature of the collector was measured using a K-type thermocouple cemented into a hole near the top of the collector base using a thermally conductive epoxy. The temperature was controlled using an Omega CNI8C PID temperature controller. The accuracy of the thermocouple-collector assembly was better than ± 0.7 K as determined by measuring the temperature when the collector was immersed in an ice bath or in boiling water. The accuracy of our temperature measurement has also been tested by comparing the observed melting temperature for azelaic acid (the C_9 diacid) to the literature value ($T_m = 380$ K) when the sample is heated at ~ 5 times the typical rate used in the TPD experiments.⁴³ For azelaic acid in our system, $T_m = 380.1 \pm 0.4$ K, in good agreement with the literature value. Such an agreement also indicates that the sample is in thermal equilibrium with the collector plate. The entire collector assembly was mounted in a glass cell maintained at 393 K attached to the back end of the ion drift tube. As molecules evaporated from the collector surface, they were directly entrained into the drift tube carrier gas flow.

Although PT-CIMS is a relatively “soft” ionization method, some of the diacids studied here exhibited significant fragmentation, often giving 2–5 mass fragments that each contributed $> 10\%$ to the total signal. The fragmentation for a given compound was characterized by comparing a background mass spectrum to one with the diacid sample heated to give observable signals. Subsequent experiments were conducted where only the identified ion fragments were monitored (typically 3–10 individual m/z).

Each TPD experiment consisted of collecting aerosol at ~ 263 K. After collection, the sample was “preheated” for 30–60 min to a temperature that was ~ 15 – 20 K below the temperature at which the maximum evaporation rate was observed (T_{max} , see Table 1). Up to $\sim 50\%$ of the originally deposited sample was lost during the preheating step. Preheating was determined to be crucial for obtaining consistently reproducible and accurate results, as discussed in detail later. After preheating, the sample was cooled to 273 K, and the TPD scan was begun after all signals recovered to background; typically, this took ~ 30 min and depended on the compound under study. A TPD scan consisted of ramping up the temperature of the collector at a rate of ~ 1.5 – 3.5 K/min while monitoring the signal levels of the various ion fragments. We observed our results to be independent of the heating rate over this range. All samples appeared to remain solid throughout the TPD scan and were completely desorbed before the melting temperature was reached.

When $[R] \ll [H_3O^+]$, as is the case here, the gas-phase concentrations of the evolved species can be calculated from the observed signals:

$$[R] = \frac{S_{R^+}}{S_{H_3O^+} \epsilon(R^+) k_{\text{rxn}} t} \quad (2)$$

where S_{R^+} is the observed signal level of R^+ (Hz), $\epsilon(R^+)$ is the transmission efficiency of the R^+ ion relative to that of the H_3O^+ ion, k_{rxn} is the second-order rate coefficient (in $\text{cm}^3 \text{ molecule}^{-1} \text{ s}^{-1}$) for the proton-transfer reaction and t is the reaction time in the ion drift tube (in seconds). For the dicarboxylic acid species it is probably reasonable to assume that the proton-

TABLE 1: Experimentally Determined ΔH_{sub}^0 , ΔS_{sub}^0 , and p^0 (298 K) for the Straight-Chain Dicarboxylic Acids, after Application of the Simple Sticking Correction^a

compound	ΔH_{sub}^0 (kJ/mol)	ΔS_{sub}^0 (J/(mol·K))	p^0 (298 K) (Pa)	T_{onset} (K)	$\sim T_{\text{max}}^*$ (K)	n	m/z
succinic acid	128 ± 2	247 ± 6	3.2 (±0.6) × 10 ⁻⁵	318	358	5	<i>101, 119</i>
glutaric acid	134 ± 4	279 ± 14	1.2 (±0.6) × 10 ⁻⁴	313	349	4	<i>87, 115, 133</i>
adipic acid	145 ± 5	285 ± 14	2.6 (±1.0) × 10 ⁻⁶	328	368	13	<i>55, 83, 101, 111, 129, 147</i>
pimelic acid	153 ± 4	313 ± 11	3.9 (±0.6) × 10 ⁻⁶	328	363	6	<i>69, 97, 115, 125, 143, 161</i>
suberic acid	168 ± 7	338 ± 18	1.8 (±1.2) × 10 ⁻⁷	348	378	9	<i>83, 101, 129, 139, 157, 175</i>
azelaic acid	178 ± 5	368 ± 16	1.0 (±0.6) × 10 ⁻⁸	348	373	15	<i>83, 97, 125, 143, 171, 189</i>
sebacic acid	181 ± 8	361 ± 22	1.6 (±0.8) × 10 ⁻⁸	353	385	13	<i>83, 101, 129, 139, 157, 185, 203</i>
dodecanedioic acid	169 ± 4	328 ± 12	3.4 (±1.1) × 10 ⁻⁸	346	377	4	<i>185, 213, 231</i>

^a The reported values are the average of n independent measurements and the errors are 2 standard deviations. The individual ΔH_{sub}^0 and ΔS_{sub}^0 were determined by fitting the data from the onset temperature (T_{onset}), where signals are first observed significantly above background, to the maximum desorption temperature (T_{max}). The diacid fragments that contributed at least 5% to the total signal are given; those that contributed >10% are italicized. The exact value of T_{max} depends on how much sample was deposited for each experiment.

transfer reaction proceeds at the gas-kinetic limit with $k_{\text{rxn}} \sim 3 \times 10^{-9} \text{ cm}^3 \text{ molecules}^{-1} \text{ s}^{-1}$.^{44,45}

The transmission efficiency of ions through the quadrupole mass spectrometer is a function of m/z . Quantitative determination requires characterization of how the relative transmission efficiency varies with m/z . This was determined for our system by completely (or nearly completely) converting the reagent ion signals (H_3O^+ and $\text{H}_2\text{O}\cdot\text{H}_3\text{O}^+$) to R^+ by controlled addition of sample compounds with various m/z . Compounds were chosen such that fragmentation and clustering were minimal, and $\epsilon(m/z)$ was determined by comparison of the decrease in the reagent ion signal to the increase in R^+ .⁴⁶

Data Analysis

Determination of Evaporation Rates and Vapor Pressures.

The evaporation rate, E (in units of molecules/s), was measured directly as a function of the desorption temperature during each TPD scan. The total amount of evaporated material (N_{tot}) was determined by integrating under the observed TPD scans:

$$N_{\text{tot}} = \int_{t=0}^{\infty} E(t) dt = \delta T^{-1} \cdot \int_{T_{\text{low}}}^{T_{\text{high}}} E(T) dT \quad (3)$$

where δT is the heating rate (K/s). Alternatively, N_{tot} was determined from the observed sample dimensions (i.e., from the initial d and h , assuming a conical shape) according to

$$N_{\text{tot}} = \rho V_0 = \frac{1}{3} \rho \pi r_0^2 h_0 \quad (4)$$

where ρ is the molecular volume and V_0 , h_0 , and r_0 are the initial sample volume, height, and radius, respectively. The two methods of determining N_{tot} typically agreed within a factor of ca. 2. For those few cases where agreement was poorer (possibly due to day-to-day fluctuations in $\epsilon(\text{X}^+)$), $E(T)$ was scaled by a constant factor to bring the two into agreement. The implications of uncertainties in N_{tot} (really in $\epsilon(\text{R}^+)$, k_{rxn} and t) in terms of the effect on the derived thermodynamic parameters are discussed further below.

The observed $E(T)$ is related to the absolute vapor pressure of a compound through the Hertz–Knudsen equation:⁴⁷

$$J_e = \frac{E}{\text{SA}} = \frac{\gamma_e p^0}{\sqrt{2\pi m k T}} \quad (5)$$

Here, J_e is the evaporation flux (molecules $\text{m}^{-2} \text{ s}^{-1}$), p^0 is the saturation vapor pressure (Pa), m is the molecular mass of the evaporating species (kg/molecule), k is Boltzmann's constant, T is temperature, and SA is the exposed sample surface area (m^2). γ_e is the so-called evaporation coefficient, which is an

empirical parameter that takes into account any energetic or entropic barrier that causes the observed evaporation flux to be less than the theoretical maximum. We make the generally accepted assumption that $\gamma_e = 1$ for the compounds considered here,^{48–50} which means that the derived vapor pressures are lower limits. The mass accommodation coefficient itself could be less than unity, but this is not considered here. Because the molecules are evaporating into a low-pressure environment, there are no diffusional constraints that would reduce the evaporation flux. As a test of this, we have measured the evaporation flux of adipic acid at a constant temperature while varying the system pressure by nearly a factor of 2. No systematic dependence of the evaporation flux on pressure was observed, and the variation between these pressure-dependent measurements was small (less than 6%).

To determine vapor pressures from the observed evaporation rates, it is necessary to have knowledge of how SA varies with temperature. The initial surface area, SA_0 , was determined from N_{tot} at $t = 0$, the molecular volume and the measured r_0 using the observation that the collected samples are cone shaped. Using these parameters, h_0 was calculated from eq 4, and $\text{SA}_0 = \pi r_0 \sqrt{r_0^2 + h_0^2}$. $V(T)$ was characterized in terms of the decreases in both r and h . In particular, it was assumed that the volume change results from simultaneous equivalent decreases in both r and h , such that $r_{t+1} = r_t \cdot f^{1/3}$ and $h_{t+1} = h_t \cdot f^{1/3}$, where f is the fraction of material remaining compared to the previous time step ($f = 1 - E_t \cdot \Delta t / N_t$). The volume calculated in this manner corresponds exactly to that calculated from the observed evaporation rates, where $V_t = V_0 - \rho \int_{t=0}^t E(t) dt$. Thus, SA can be specified at every T (from r_t and h_t), and the measured $E(T)$ can be converted to $J_e(T)$. We have also visually monitored the sample during a TPD scan and found that the observed variation in r and h (and SA) with temperature agreed very well with the calculated values, typically to better than 10% at any given temperature. We therefore have confidence that the variation in SA with temperature has been accounted for properly.

$p^0(T)$ was calculated using eq 5 from the measured $J_e(T)$. Over a limited temperature range, a plot of $\ln p^0$ vs $1/T$ is linear with a slope equal to $\Delta H_{\text{sub}}^0/R$ and an intercept equal to $\Delta S_{\text{sub}}^0/R$ (i.e., Clausius–Clapeyron equation), where R is the ideal gas constant and ΔS_{sub}^0 is the entropy of sublimation.⁵¹ (This assumes that $\Delta C_p = 0$, i.e., that ΔH_{sub}^0 does not vary significantly over the temperature range considered.) The vapor pressure at 298 K was calculated for comparison with other values found in the literature from the measured ΔH_{sub}^0 and ΔS_{sub}^0 . This method provides a direct measure of the compound vapor pressure as a function of temperature, within the constraints of the Hertz–Knudsen formulation for evaporation (i.e., assuming $\gamma_e = 1$).

Each observed TPD curve was compared to a model curve, which has ΔH_{sub}^0 and ΔS_{sub}^0 as the only two adjustable parameters. The model was initialized using the observed N_{tot} and r_0 to establish SA_0 . At every time (temperature) step in the model, E was calculated from eq 5 and the incremental mass loss determined. The molecules evaporated during that time step are removed from the sample and the r and h (and SA) for the next time step determined in the same manner as above. This process was continued until $N_i = 0$.

High Temperature Correction. In some of the experiments, significant high-temperature “tailing” was observed, where the gas-phase concentration decreased less rapidly than estimated from earlier time measurements or expectations from the model (cf. Figure 2). However, the following observations suggest that this slow signal decay was most likely due to evaporation from the walls of the ion drift tube and not from residual sample on the collector plate. Visual inspection of the sample during a TPD scan indicated that the sample was completely evaporated once the temperature was ca. 5 K higher than T_{max} . Additionally, the diacid signal persisted after T_{max} was reached even when the collector plate was rapidly cooled to temperatures where there was negligible evaporation. This observation provides confidence that our interpretation of the tailing to be the result of sticking downstream from the desorption region is correct. The high-temperature tail generally contributes 5–15% of the total signal.

To approximately account for the high-temperature tailing, the data were corrected as follows. First, the total area under the observed curve, A_{observed} , including the tail, was determined. Then, when the actual temperature was above some high-temperature cutoff (T_{cutoff}) the observed signals were adjusted such that $S(t+1) = 0.5 \cdot S(t)$. This is equivalent to assuming that the actual high-temperature decay is exponential with time. The value of T_{cutoff} was determined from the experiments when the conditions were such that $T > T_{\text{max}}$ and $S_X(T) < 0.4 \cdot S(T_{\text{max}})$. Application of this scaling factor effectively removes the tailing and provides for excellent correspondence with the model in the high-temperature falloff region of the TPD curve. The scaling factors (0.4 and 0.5) were empirically determined to yield best agreement with the visual observations and with the model. Each of the S_X of the tailing-corrected curve were multiplied by the ratio $A^* = A_{\text{observed}}/A_{\text{scaled}}$ such that N_{tot} was conserved.

It is important to consider how the application of this sticking correction affects the derived ΔH_{sub}^0 , ΔS_{sub}^0 , and $p^0(298 \text{ K})$. Recall that, to extract vapor pressures from the observed evaporation rates, it is necessary to know $SA(T)$. When we do not account for sticking, the determined $SA(T)$ is incorrect because sample apparently remains on the collector at $T \gg T_{\text{max}}$. Without correction the apparent SA at every temperature is therefore slightly larger than the actual SA , and the derived p^0 is correspondingly too low because $p^0 \propto SA^{-1}$. The exact magnitude of the deviation is a function of temperature because SA changes nonlinearly with T . When the sticking correction is applied, SA changes in accord with expectations from the visual observations of the sample and from the model; the sample is effectively completely evaporated for $T > T_{\text{max}} + \sim 5 \text{ K}$.

Slightly larger R^2 values are typically found in the linear fits to plots of $\ln p^0$ vs $1/RT$ when the corrections for sticking are applied, although both typically have $R^2 > 0.99$. However, the corrected data (as $\ln p^0$ vs $1/RT$) is highly linear from the signal onset temperature up to T_{max} , whereas the uncorrected data must be fit over a more limited temperature range or significant

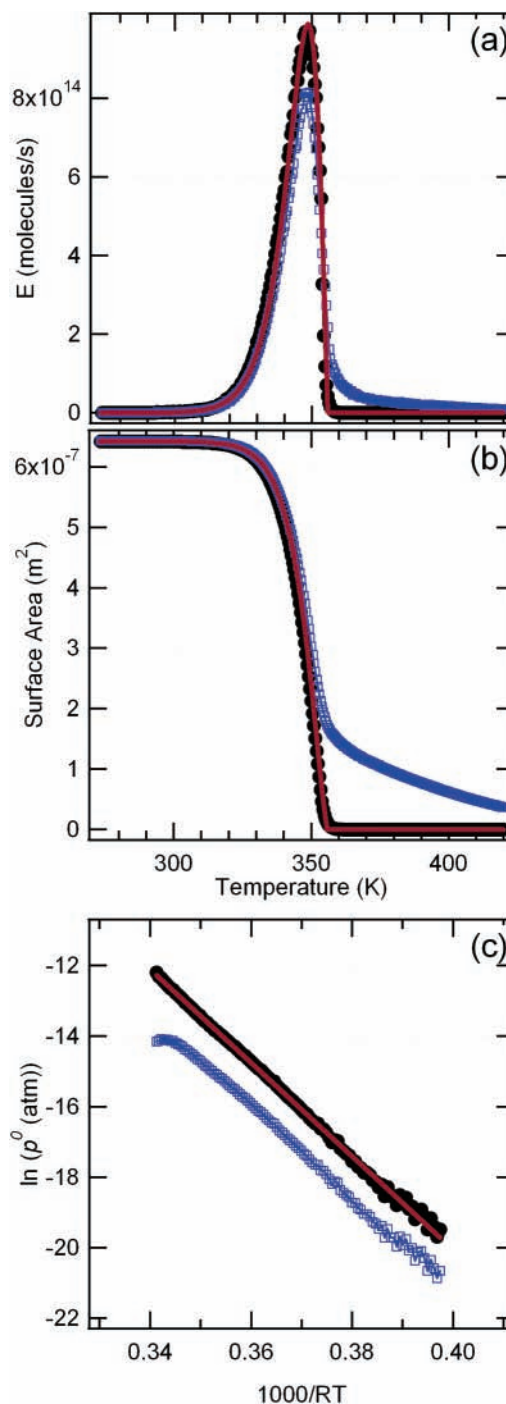


Figure 2. (a) Typical TPD scan for glutaric acid with the uncorrected (\square , blue line), sticking/tailing-corrected (\bullet , black line), and model data ($-$, red line). (b) Corresponding calculated variation in the sample surface area with the desorption temperature. (c) $\ln p^0$ vs $1000/RT$. The line is the best fit to the corrected data. When the correction is not applied, the curve begins to deviate significantly from linear as T_{max} is approached, and therefore the fit was performed over a smaller range than shown. The uncorrected data have been offset by -1 for visual clarity. Note the different x-axis for (c).

curvature in the $\ln p^0$ vs $1/RT$ plots are observed. The correction generally leads to an increase in ΔH_{sub}^0 of 1–5 kJ/mol and a change in $p^0(298 \text{ K})$ of $< 15\%$, with no systematic dependence on N_c . Note that if ΔS_{sub}^0 is held constant while ΔH_{sub}^0 is changed by 5 kJ/mol, the calculated $p^0(298 \text{ K})$ can change by nearly an order of magnitude. This indicates that both ΔH_{sub}^0 and ΔS_{sub}^0 change so as to keep $p^0(298 \text{ K})$ approximately constant.

Because a constant scaling factor has been used above, the increase in the derived ΔH_{sub}^0 after correction arises solely due to changes in $SA(T)$, i.e., in the conversion from $E(T)$ to $p^0(T)$. Consideration instead of a temperature/time dependent correction indicates that the constant correction used above may still underestimate the true ΔH_{sub}^0 (see Supporting Information). However, the $p^0(298\text{ K})$ determined using the temperature dependent correction are typically decreased by $<10\%$ from the constant correction values. Clearly, sticking is an experimental problem that causes some error, although the effect on the derived $p^0(298\text{ K})$ appears to be relatively minor.

Results and Discussion

Measurements of evaporation rates of the C_4 – C_{10} and C_{12} straight-chain dicarboxylic acids were made using the TPD-PT-CIMS system. From these measurements, ΔH_{sub}^0 , ΔS_{sub}^0 , and $p^0(298\text{ K})$ were determined for each diacid, after the constant sticking correction was applied (Table 1). All reported errors are 2 standard deviations as determined from at least 4 independent measurements. A representative TPD scan is shown for glutaric acid (the C_5 diacid) (Figure 2a), along with the determined $SA(T)$ (Figure 2b). The original, uncorrected evaporation rates are shown for comparison. Also shown is a plot of $\ln p^0$ vs $1/RT$ from which the thermodynamic parameters ΔH_{sub}^0 and ΔS_{sub}^0 were determined at a standard state of 1 atm (Figure 2c). Typically, no signal is observed until ~ 310 – 350 K due to sensitivity limitations of the PT-CIMS system. For this particular trial, application of the sticking correction produces a change in ΔH_{sub}^0 from 131.1 to 134.3 kJ/mol and in the extrapolated $p^0(298\text{ K})$ from 1.1×10^{-4} to 1.2×10^{-4} Pa. ΔH_{sub}^0 increases to 136.0 kJ/mol and $p^0(298\text{ K})$ decreases to 1.05×10^{-4} Pa when the temperature-dependent sticking correction is applied. Application of the sticking correction primarily engenders changes in ΔH_{sub}^0 but leaves $p^0(298\text{ K})$ relatively unaffected. This is likely because the model best retrieves $p^0(298\text{ K})$, rather than ΔH_{sub}^0 and ΔS_{sub}^0 , because of the compensation between these two quantities and the limited T -range.

The experimentally determined $p^0(298\text{ K})$ vary in a strongly nonmonotonic manner with N_c ; vis., there is an “odd–even” dependence observed with respect to N_c (Figure 3). This odd–even alternation in $p^0(298\text{ K})$ has previously been noted for the straight chain dicarboxylic acids.^{17,20} This observation has been rationalized by analogy to measurements of the melting temperature, T_m , of the diacids,¹⁷ where a strong odd–even dependence is observed; the odd diacids typically melt at lower temperatures than the even diacids.^{52,53} We note, however, that $p^0(298\text{ K})$ for the C_{12} diacid is greater than that for the C_{10} diacid, different to the variation observed between the smaller even carbon number diacids.

In contrast to $p^0(298\text{ K})$, both ΔH_{sub}^0 and ΔS_{sub}^0 increase approximately monotonically with N_c up to C_9 such that no odd–even effect is readily discernible (Figure 4). However, because $p^0(298\text{ K})$ was determined from ΔH_{sub}^0 and ΔS_{sub}^0 , the small differences in these properties between adjacent carbons (e.g., in going from C_5 to C_6) must depend on whether an odd–even or even–odd step is considered. In other words, because there is a strong odd–even dependence in the derived $p^0(298\text{ K})$ there must be an odd–even dependence in $\Delta H_{\text{sub}}^0 - T\Delta S_{\text{sub}}^0$, even if the odd–even dependencies for ΔH_{sub}^0 and ΔS_{sub}^0 are almost indiscernible. The ΔH_{sub}^0 and ΔS_{sub}^0 for the C_{12} diacid are actually significantly lower than for C_{10} , indicating that the nearly linear trend in N_c suggested by the smaller diacids cannot

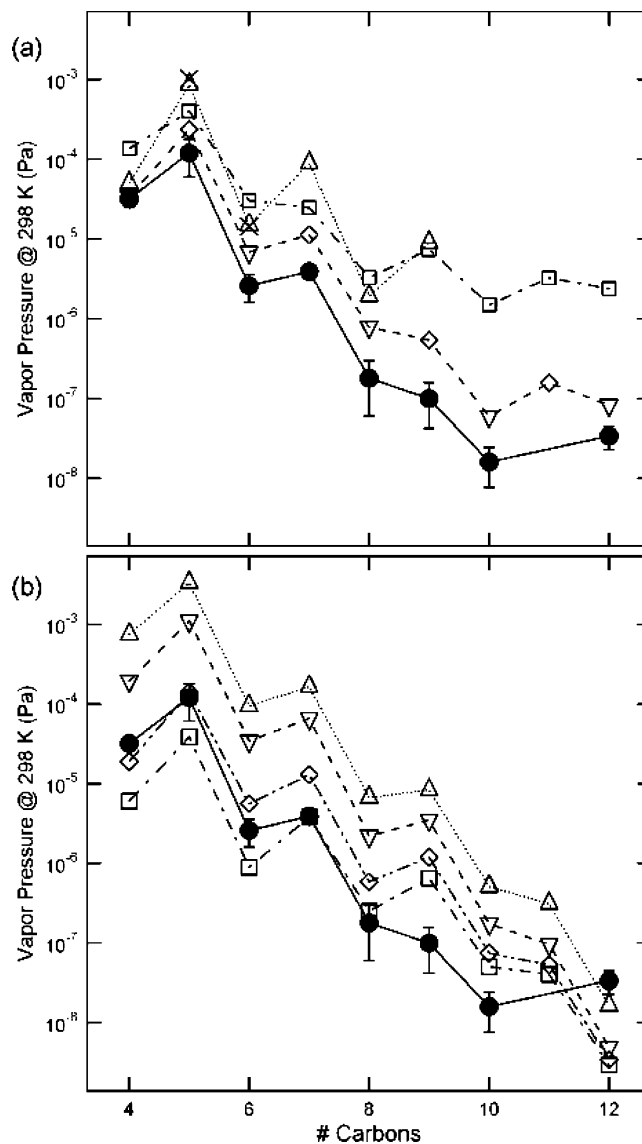


Figure 3. (a) Measured vapor pressures (Pa) for the straight-chain diacids for this work (●), Bilde et al.¹⁷ (△), Chattopadhyay and Ziemann²⁰ (□), Tao and McMurry¹⁶ (×), da Silva et al.¹⁴ (◇), and Davies and Thomas¹³ (▽). (b) Measured vapor pressures for this work compared to calculated values from SPARC²⁵ (□), Capouet and Müller⁴¹ (△), and UNIFAC using the parameters from either Jensen et al.²³ (◇) or Asher et al.²⁴ (▽). The 2σ error bars for this work are shown. Note that the y-axis is a log scale.

simply be extrapolated to predict the properties of the larger diacids. Previous measurements^{17,20} indicated that there is a strong odd–even dependence in ΔH_{sub}^0 , in contrast to the results presented here. There is a clear odd–even dependence in both the enthalpy and entropy of fusion for these compounds,⁵⁴ and it is therefore of interest that our results indicate that ΔH_{sub}^0 and ΔS_{sub}^0 exhibit only, at most, a weak odd–even dependence.

Role of Preheating and Effect of Solvent. It is important to consider the strong influence that preheating of the sample has on the determined thermodynamic parameters. Two separate examples of adipic acid TPD scans with no preheating are compared with a scan where the sample was preheated for 30 min at 343 K (Figure 5). On occasion, a “bump” in the TPD curve was observed when the sample was not preheated, as exemplified by curve a. In this case, it is likely that a significant amount of extraneous sample was deposited as thin layers on

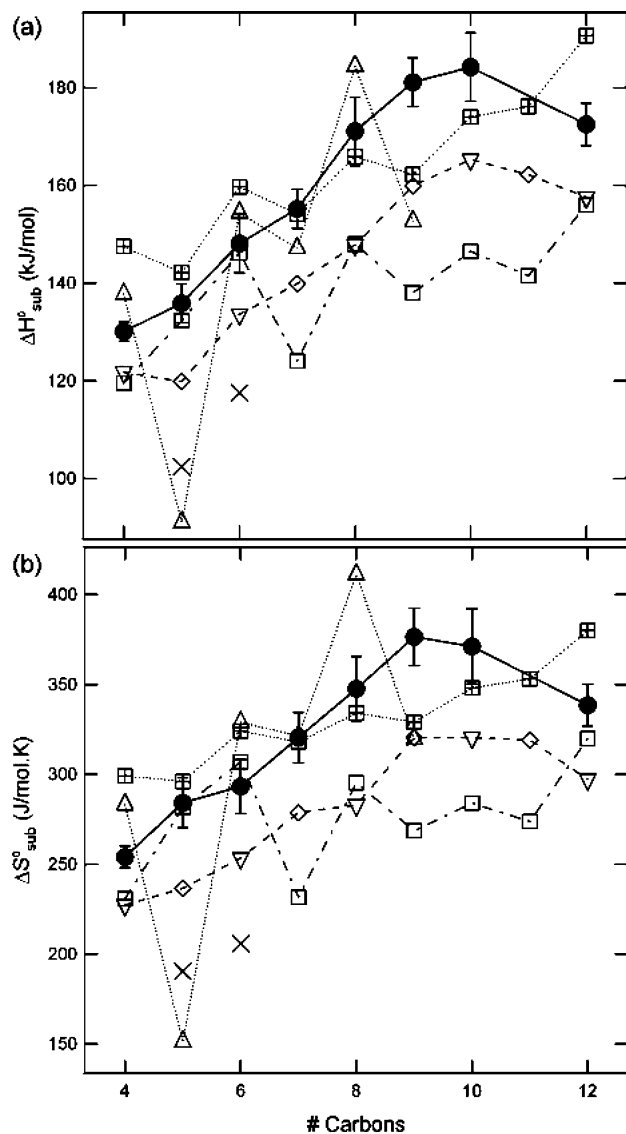


Figure 4. Measured (a) ΔH_{sub}^0 and (b) ΔS_{sub}^0 for the straight-chain diacids for this work (\bullet), Bilde et al.¹⁷ (Δ), Chattopadhyay and Ziemann²⁰ (\square), Tao and McMurry¹⁶ (\times), da Silva et al.¹⁴ (\diamond), and Davies and Thomas¹³ (∇) and calculated values from SPARC²⁵ (\boxplus). Note that the da Silva and Davies and Thomas data have been connected with a single line. The 2σ error bars for this work are shown.

the collector and that this sample desorbed at lower temperatures, resulting in the observed bump. The presence of extraneous sample will increase the observed evaporation rates at lower temperatures due to the added surface area for evaporation, but as the extraneous sample is depleted and the surface area reduced, the contribution will decrease. Curve b shows another example with no preheating, but where no such bump was observed. The observed $E(T)$ for this trial were excessively large, particularly at lower temperatures, in comparison to the preheated trials. Consequently, the derived $p^0(298\text{ K})$, ΔH_{sub}^0 , and ΔS_{sub}^0 were significantly different between the preheated and not preheated trials, specifically with $p^0(298\text{ K})$ larger and ΔH_{sub}^0 smaller when samples were not preheated (Figure 6). This result holds generally true for all of the diacids considered here, although the magnitude of the discrepancy between the preheated and not preheated parameters increases with increasing N_c (Figure 7). Interestingly, the $p^0(298\text{ K})$ determined for the not preheated trials are well within the scatter of the previous measurements, exhibiting overall good agreement. This suggests

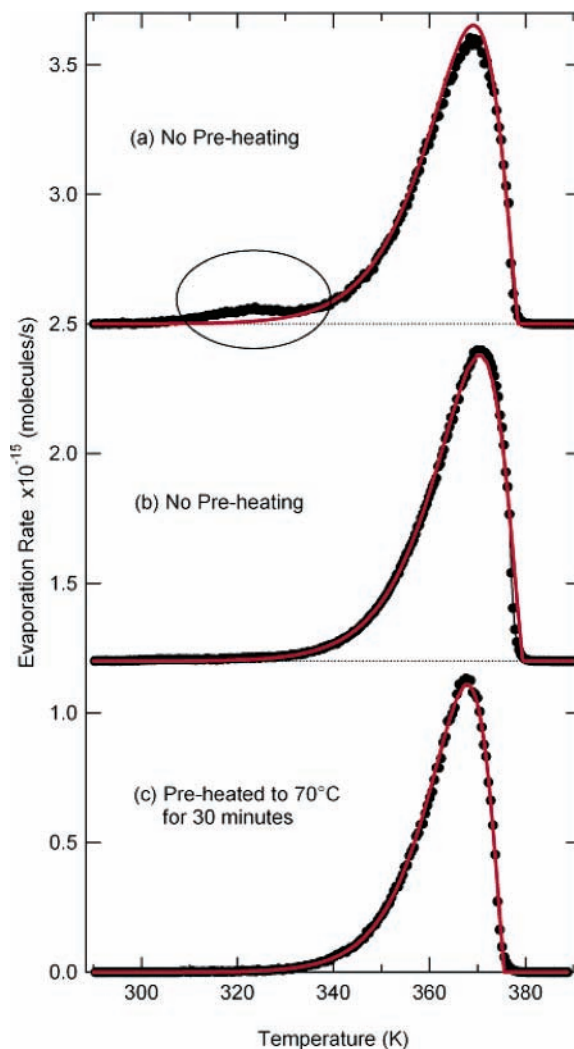


Figure 5. (a) Example TPD scan of adipic acid where no preheating step was performed. Note the anomalous increase in E that occurs around 60°C . This “bump” is due to desorption of significant amounts of extraneous sample from the collector. (b) Second example with no preheating step, but where no obvious low-temperature “bump” was observed. After the “bump” (a) and (b) are very similar. (c) Example of a preheated adipic acid TPD scan. Compared to the not preheated trials, the $p^0(298\text{ K})$ and ΔH_{sub}^0 is larger. Considering (b) and (c), the preheated parameters ($p^0(298\text{ K})$, ΔH_{sub}^0 , and ΔS_{sub}^0) were $3.2 \times 10^{-6}\text{ Pa}$, 142 kJ/mol , and $275\text{ J/(mol}\cdot\text{K)}$, compared to not preheated values of $1.4 \times 10^{-5}\text{ Pa}$, 126 kJ/mol , and $233\text{ J/(mol}\cdot\text{K)}$. All data have been corrected for sticking. Data are shown as black circles, and the model fits, as red lines.

that preheating is likely the primary reason for the generally lower $p^0(298\text{ K})$ values observed in this study.

Both the preheated and not preheated data can be fit surprisingly well by the model (when no “bump” is observed) so it is not possible to establish the “correctness” of one over the other on the basis of the fit alone. However, we believe the preheating step to be essential to obtaining correct results. Importantly, we suspect that this preheating discrepancy does not arise solely from evaporation of extraneous sample, but from conditioning of the sample prior to desorption as well. Recall that the deposited aerosols are generated by nebulizing a 1–2 wt % diacid in methanol solution to produce aerosols, which are sent through a drier to remove much of the methanol. However, upon deposition the aerosols are not 100% dry and may still contain significant amounts of methanol. Although methanol itself would not be efficiently trapped at the collector

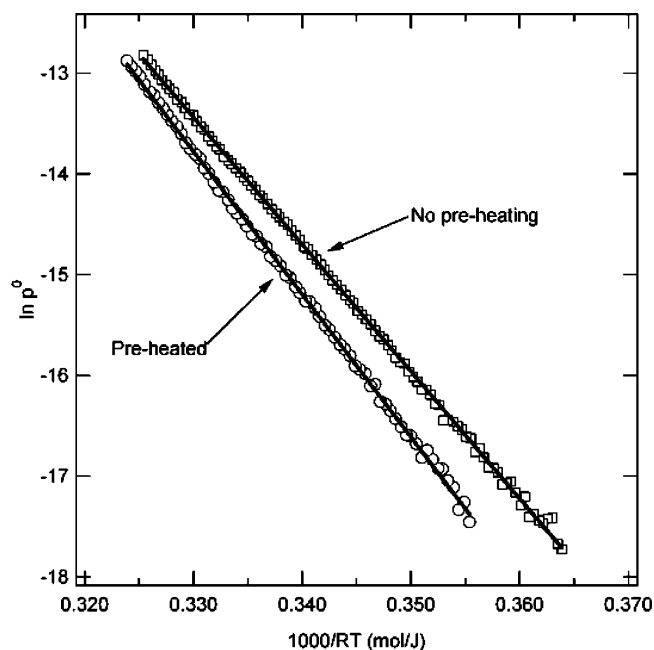


Figure 6. $\ln p^0$ vs $1000/RT$ (with 1 atm as the standard state) as determined from the preheated (●) and not preheated (□) scans shown in Figure 5. Note that both give excellent linear fits.

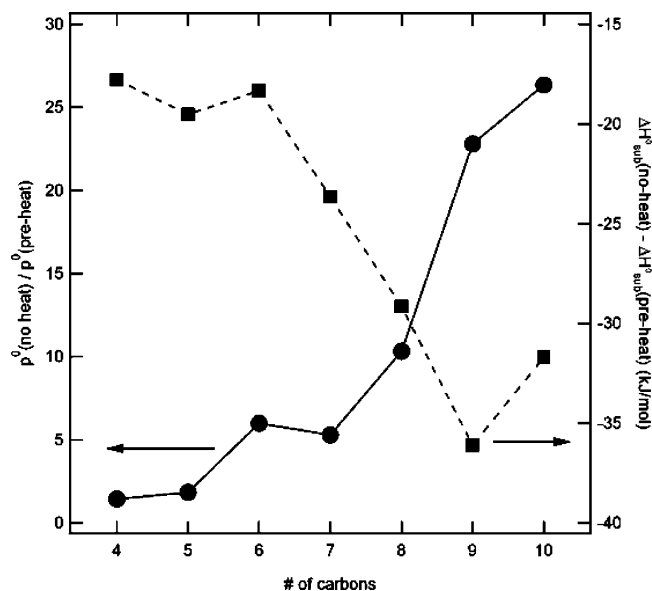


Figure 7. Ratio between the $p^0(298\text{ K})$ (left axis, ●) and the difference in ΔH_{sub}^0 (right axis, ■) as determined from the experiments with no preheating step and those with preheating, as a function of N_c .

temperature, if trapped within the bulk of the deposited solid sample it would likely influence the observed evaporation rates. We might expect that methanol would tend to *increase* the observed E at a given temperature and *decrease* the determined ΔH_{sub}^0 because the vapor pressure for methanol is orders of magnitude higher and ΔH_{sub}^0 significantly lower than for the diacids, consistent with the observations. The preheating step may serve to drive the highly volatile methanol out of the collected sample (as well as remove any volatile surface impurities and extraneous sample), thereby allowing for measurement of the thermodynamic properties of the purified diacids. It was noted by Davies and Thomas that, for their Knudsen cell effusion experiments, “not infrequently the first points obtained with a new acid showed abnormally high

pressures due, it seems certain, to the early loss of volatile impurities (moisture).”¹³

In fact, during the preheating step, the methanol signal exhibits a sharp increase immediately upon heating, while there is a delay in the diacid signal increase. After preheating, the diacid signal decreases with temperature whereas the methanol signal remains constant at the background value (see Figure S1a in the Supporting Information). This suggests that methanol has been desorbed from the sample during the preheating step. Also, no change in the methanol signal during the TPD scan is observed after preheating; i.e., no methanol is co-desorbed with the evaporating diacid sample (see Figure S1b). In contrast, the methanol signal increases as a TPD scan progresses for the not preheated samples, although it does not necessarily follow the diacid signals exactly. If the primary difference between the preheated and not preheated trials is the presence of methanol in the samples, rather than desorption of extraneous sample (which, however, may lead to the sometimes observed “bump”), this may explain why both give linear fits to a plot of $\ln p^0$ vs $1/RT$. We have observed a similar preheating/no-heating discrepancy when either water or 1-propanol is used as the solvent, although we note that for 1-propanol there appears to be an additional dependence upon the age of the solution where, after a few hours, different results are obtained compared to fresh solutions. The reason for this age dependence is, as yet, unexplained.

The amount of methanol retained in the deposited adipic acid sample was estimated from the observed methanol signals during preheating. From the data shown in Figure S1a, we have determined that $\sim 5\%$ of the total deposited sample was methanol. The small relative abundance of methanol in the sample suggests that the different thermodynamic properties measured for the preheated vs not preheated trials does not arise from a direct interaction of every diacid molecule with a solvent molecule. Instead, we speculate that the primary influence of the solvent molecules is to disrupt the crystal structure at the evaporating surface, thereby allowing many of the diacid molecules at the surface to exist in configurations from which evaporation is more likely than in the purified samples.

An additional potential explanation for the observed influence of preheating is sintering of the sample. Sintering during preheating would likely have led to a decrease in the surface roughness and porosity, thereby decreasing the actual surface area, which might be somewhat greater than the geometric surface area and which we have used here. It is also possible that the deposited aerosol particles were actually agglomerates of very small crystals, for which the Kelvin effect might be important, although we believe this to be less likely given the observations. As a result of this change in effective surface area, sintering would have caused the observed evaporation rates after preheating to be lower than those without preheating, consistent with our results. However, it is unlikely that sintering alone would lead to the observed factor of >20 decrease in the evaporation rates and vapor pressures of the longest diacids. Additionally, the enthalpy of sublimation should be unaffected by sintering, in contrast with our observations. As a final consideration, we mention that no significant changes in the measured mass spectra were observed upon preheating, which indicates that thermal degradation or chemistry (e.g., esterification reactions) were unimportant. Thus, we believe that the effect of preheating is primarily due to the influence of residual solvent, as described above, although sintering may contribute somewhat to the observed decrease in vapor pressures with

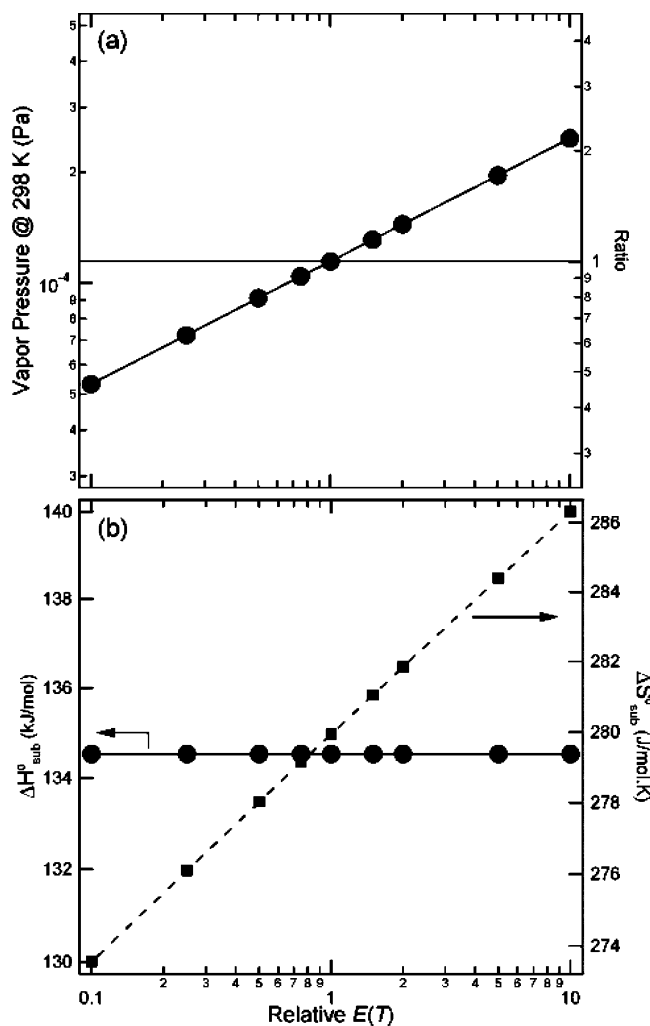


Figure 8. Sensitivity analysis of (a) $p^0(298\text{ K})$ and (b) ΔH_{sub}^0 (left axis, ●) and ΔS_{sub}^0 (right axis, ■) to uncertainties in the measured $E(T)$. The derived vapor pressures change by only a factor of 2 for changes in $E(T)$ of a factor of 10 as a result of corresponding changes in the surface area.

preheating. Measurement of the BET surface area of unheated and preheated samples in the future would help address this issue.

Sensitivity Analysis. The errors reported in Table 1 are an indication of the precision of the measurements. The accuracy is primarily limited by the suitability of the cone surface area model and the measurement of $E(T)$. The uncertainty in E is determined, to a significant extent, by the relative mass spectrometer transmission function correction, but also by uncertainties in k_{rxn} and t . However, the total effect of uncertainties in the measured evaporation rate is limited because the total sample mass is well constrained by the visually determined size. It is nonetheless useful to assess the sensitivity of the extracted $p^0(298\text{ K})$, ΔH_{sub}^0 , and ΔS_{sub}^0 to potential errors in $E(T)$. To do this, the measured $E(T)$ were scaled by a temperature-independent constant, and the corresponding sample size was constrained such that $h_0 = d_0$. (If this constraint is not applied, such that either the base diameter or cone height is constant with $E(T)$, then physically unreasonable cone shapes are obtained.) The changes in $p^0(298\text{ K})$, ΔH_{sub}^0 , and ΔS_{sub}^0 were then assessed. The results of this analysis are shown in Figure 8 using the glutaric acid TPD scan shown in Figure 2 as an example. Errors in measurement of $E(T)$ have essentially no effect on the derived ΔH_{sub}^0 , within the constraints of the

simple sticking correction; only the ΔS_{sub}^0 are affected, and through them the $p^0(298\text{ K})$. Interestingly, increasing (decreasing) $E(T)$ by a factor of 10 leads to an increase (decrease) in the determined $p^0(298\text{ K})$ of only a factor of ca. 2. Thus, to increase the derived $p^0(298\text{ K})$ by a factor of ca. 10 or more (to obtain approximate agreement with some of the other measurements) would require extremely unrealistic uncertainties in the measured $E(T)$. We estimate that N_0 for a given measurement is known to within at worst 50%, resulting in a maximum error in $p^0(298\text{ K})$ of $\sim 15\%$, which is typically smaller than the precision based uncertainty.

We have also tested the applicability of the cone model by treating the sample as either a cylinder or a half-sphere. This analysis indicates that ΔH_{sub}^0 is unaffected by the chosen shape of the sample. $p^0(298\text{ K})$ changes by only a small amount, with $p^0(298\text{ K})$ values of 1.15×10^{-4} , 1.07×10^{-4} , and 1.28×10^{-4} Pa for the cone, cylinder, and sphere models, respectively. Such small changes in the determined parameters with sample shape can be rationalized by recognizing that there is a negligible difference in how SA varies with temperature between these three shapes.

We have also explored the assumption that the volume decrease is from equivalent changes in d and h by allowing the volume change to result from variation only in d or only in h . In either case, there is a strong change in the shape of the calculated $E(T)$, but the resulting changes in the derived thermodynamic parameters are small. For this example, ΔH_{sub}^0 decreases from 134.5 to 132.5 or 133.9 kJ/mol, and $p^0(298\text{ K})$ increases negligibly from 1.15×10^{-4} to 1.22×10^{-4} or 1.18×10^{-4} Pa, for variation only in d or h , respectively. It is evident the most important factor is that SA varies with temperature; the actual shape of the sample is secondary. Thus, our results are robust with respect to the use of the cone model.

Comparison to Literature Values of $p^0(298\text{ K})$, ΔH_{sub}^0 , ΔS_{sub}^0 . The derived $p^0(298\text{ K})$ from this work and from previous experiments^{13,14,16,17,20} (Figure 3a) and those calculated with group-contribution methods^{23–25,41} (Figure 3b) are shown. The calculated liquid phase $p^0(298\text{ K})$ were converted to solid phase $p^0(298\text{ K})$ values through the relationship²⁶

$$\ln p_s^0(T) = \ln p_L^0(T) - \left[\frac{\Delta S_{\text{fus}}(T_m)}{R} \left(\frac{T_m}{T} - 1 \right) \right] \quad (6)$$

where the subscript s and L stand for the solid and liquid phases, respectively, and $\Delta S_{\text{fus}}(T_m)$ is the entropy of fusion at the melting point. ΔS_{fus} and T_m values are from NIST.⁴³ We note that the p_s^0 values calculated here from the SPARC p_L^0 are significantly lower than the p_s^0 obtained directly from the SPARC online website.⁵⁵ The reason for this discrepancy is unclear. Also, the p_s^0 determined from UNIFAC^{21,22} depend upon whether the parameters of Jensen et al.²³ or of Asher et al.²⁴ are used.

The measured and literature ΔH_{sub}^0 and ΔS_{sub}^0 are shown in Figure 4. Many of the previous experimental studies did not report values for ΔS_{sub}^0 specifically, but for an integration constant, C , from the Clausius–Clapeyron relationship. We have converted these C 's to ΔS_{sub}^0 , using 1 atm as the standard state. To facilitate comparison with previous measurements, we have converted our measured values to standard values at 298 K according to⁵⁶

$$\Delta H_{\text{vap}}^0(298\text{ K}) = \Delta H_{\text{vap}}^0(\langle T \rangle) + \Delta C_p[298.15\text{ K} - \langle T \rangle] \quad (7)$$

and

$$\Delta S_{\text{vap}}^0(298 \text{ K}) = \Delta S_{\text{vap}}^0(\langle T \rangle) + \Delta C_p \ln \left[\frac{298.15 \text{ K}}{\langle T \rangle} \right] \quad (8)$$

ΔC_p is the standard molar heat capacity of sublimation (assumed to be temperature independent), and $\langle T \rangle$ is the average temperature during the TPD measurement. We use $\Delta C_p = -50 \text{ J}/(\text{mol} \cdot \text{K})$,¹⁴ giving room-temperature values of ΔH_{sub}^0 and ΔS_{sub}^0 that are larger than the experimental values by $\sim 3 \text{ kJ}/\text{mol}$ and $\sim 10 \text{ J}/(\text{mol} \cdot \text{K})$, respectively.

Clearly, there is a great deal of variability in the measured and calculated $p^0(298 \text{ K})$, ΔH_{sub}^0 , and ΔS_{sub}^0 between the different studies. For example, the measured $p^0(298 \text{ K})$ values for glutaric acid vary over 2 orders of magnitude. Despite this overall variability, the $p^0(298 \text{ K})$ from this study are systematically lower than the previously reported values, often by an order of magnitude or more. This is particularly apparent for the longer chain diacids. These results suggest that the C_4 – C_{10} and C_{12} diacids will partition to the aerosol phase to a greater extent than previously suggested due to their lower vapor pressures.

The general nature of the odd–even dependence evidenced by $p^0(298 \text{ K})$ is actually very similar to that observed by Bilde et al.¹⁷ and Chattopadhyay and Ziemann²⁰ (henceforth referred to as CZ) and the combined Knudsen cell results from Davies and Thomas (even carbon numbers) and da Silva et al. (odd carbon numbers)^{13,14} (Figure 3). In general, with increasing N_c there is a slight increase or only small change in $p^0(298 \text{ K})$ when going from even to odd numbers of carbons with a comparatively larger decrease when going from odd to even. One difference is that we observe a slight decrease in going from C_8 to C_9 , whereas Bilde et al. and CZ both observed an increase.

In contrast, the variation of ΔH_{sub}^0 and ΔS_{sub}^0 with N_c observed here is quite different from some of the previous observations (see Figure 4). Bilde et al., using a TDMA method, found that ΔH_{sub}^0 exhibited an extremely large odd–even dependence. CZ, using a different TPD method, observed a comparably minor, although apparent, odd–even effect with a small overall change in ΔH_{sub}^0 in going from $N_c = 4$ to $N_c = 12$. Compared to these studies, our results exhibit a negligible odd–even effect in ΔH_{sub}^0 and ΔS_{sub}^0 .

What might be the cause of these differences? First, we note that in our experiments ΔH_{sub}^0 is determined for each trial, and the reported ΔH_{sub}^0 values are the average of numerous *independent* measurements. In the Bilde et al. experiments (where the largest odd–even dependence in ΔH_{sub}^0 was observed), each experiment yielded p^0 at a single temperature only. ΔH_{sub}^0 was determined from a best fit to a plot of $\ln p^0$ vs $1/RT$ where each $p^0(T)$ was from a *separate* experiment. As a result, the fits to the data may be subject to greater uncertainty (there are only 5–7 individual $p^0(T)$ measurements for each diacid). This is apparent if one compares, as an example, the fits shown in our Figures 2 and 6 with those shown in Figure 7 of ref 17.

Comparing to the TPD experiments of CZ, the reason for the discrepancy is less clear because they employed a method similar to ours. In the experiments of CZ on the C_5 , C_7 , and C_9 diacids, multiple desorption peaks were observed. This was attributed to the presence of different polymorphs (i.e., crystal structures) of these compounds in the deposited aerosols. The TPD profiles for these particular compounds therefore deviated significantly from their spherical particle evaporation model (which is similar to the cone model introduced here) and we speculate may have led to less than optimal fits and the apparent observation of an odd–even dependence in ΔH_{sub}^0 . There was no evidence of such multiple desorption peaks in our experi-

ments for the odd diacids for the preheated trials (see Figure S2 in the Supporting Information for representative TPD scans for all of the diacids). If polymorphs of these compounds did exist, the preheating step may have served to convert them to the more stable species so that only a single polymorph was present during the TPD scans.⁵⁷ For the not preheated trials, a few of the C_5 and C_7 diacid TPD scans showed some evidence of multiple peaks; however, the behavior of these particular samples was not reproducible and no such multiplex structure was observed for the C_9 diacid. Additionally, due to the design of the collector in the CZ experiments, sticking/redesorption of the compounds from the collector surface was also potentially quite significant. Although they made efforts to minimize this sticking, they found only a moderate agreement between the experimental data and their spherical particle model indicating that sticking was still likely contributing to their data (cf. their Figures 3 and 4). The extent to which sticking may have affected the ΔH_{sub}^0 values measured by CZ is unknown.

A separate possibility is that both the TDMA and TPD experiments of CZ were affected by the presence of solvent (used in the aerosol generation process in both experiments) trapped within the diacid matrix. Such a possibility is consistent with the observation that our $p^0(298 \text{ K})$ values are typically lower and ΔH_{sub}^0 higher than in these previous studies. As mentioned above, a solvent effect was also apparent here for water (used by Bilde et al.) and 1-propanol (2-propanol was used by CZ).

The approximately linear variation in ΔH_{sub}^0 with N_c up to $N_c = 9$ observed in our experiments is more consistent with the combined Knudsen cell results,^{13,14} although the reported values are $\sim 15 \text{ kJ}/\text{mol}$ lower than those observed here. The reason for this discrepancy is unclear. The Knudsen cell $p^0(298 \text{ K})$ values are generally larger than our $p^0(298 \text{ K})$ (with the exception of the C_4 diacid); however, they are overall closer to our results than either the TDMA¹⁷ or the other TPD²⁰ results.

Comparing our experimental $p^0(298 \text{ K})$ to the calculations from group-contribution methods, there is a strong similarity in the shapes of the observed and calculated odd–even dependence, although the calculations all suggest that $p^0(298 \text{ K})$ should increase in going from C_8 to C_9 (Figure 3b). Additionally, the calculations all indicate that $p^0(298 \text{ K})$ for the C_{12} diacid is significantly less than that for the C_{10} diacid, in contrast to the observations. With respect to absolute values, reasonable agreement is found with the $p^0(298 \text{ K})$ from SPARC²⁵ and from the Jensen-UNIFAC²³ method for $N_c \leq 8$. The $p^0(298 \text{ K})$ from this study are significantly lower in comparison both to the method of Capouet and Müller⁴¹ and to the Asher-UNIFAC method.²⁴

We believe that the discrepancy between the $p^0(298 \text{ K})$ calculated from the Jensen²³ and Asher²⁴ UNIFAC methods can be understood through consideration of the parameters themselves. Without going into detail, the combinatorial contribution to the calculated p_L^0 depends importantly on four parameters, $A_{k,1} - A_{k,4}$, through the relationship^{23,24}

$$\ln p^0(T) \rightarrow \frac{A_{k,1}}{T} + A_{k,2} + A_{k,3}T + A_{k,4} \ln T \quad (9)$$

The first two terms in eq 10 are completely negligible compared to the last two when the Asher et al. $A_{k,x}$ values are used, whereas all four terms are important when the Jensen et al. parameters are used. It is therefore possible that the $A_{k,x}$ reported by Asher et al. may only be a local minimum in the nonlinear regression used in their determination, whereas the Jensen et al. $A_{k,x}$ may be closer to a global solution.

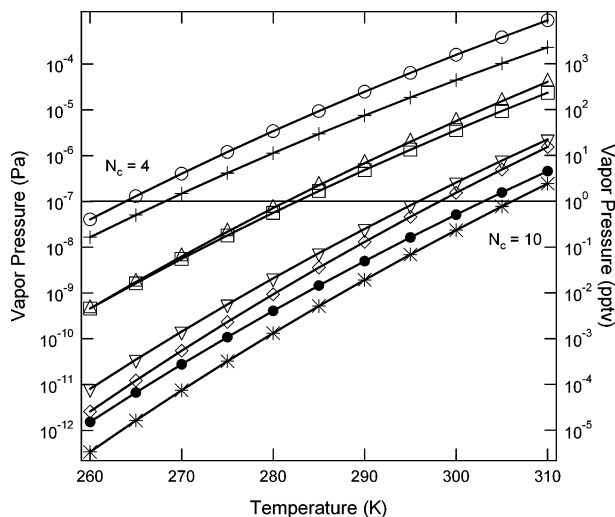


Figure 9. Temperature dependence of the saturation vapor pressures (in Pa and pptv) of the straight chain dicarboxylic acid for $N_c = 4$ to $N_c = 10$ and $N_c = 12$. Shown are succinic (+), glutaric (O), adipic (□), pimelic (Δ), azelaic (◇) and sebacic (*), acid and dodecanedioic acid (●).

Atmospheric Implications. The $p^0(298\text{ K})$ determined here for the C_4 – C_{10} and C_{12} straight-chain dicarboxylic acids are significantly lower than previous measurements or calculations indicate. Also, the vapor pressures are strongly temperature dependent, decreasing by approximately an order of magnitude for a 10 K drop in temperature. For example, at $T < 280\text{ K}$, $p^0 < 1\text{ pptv}$ (10^{-7} Pa) for all $N_c > 5$ (Figure 9). As a result, the gas-to-particle partitioning of these compounds, as determined using the Pankow model,^{8–10} may be significantly greater than previously thought. Additionally, because these types of compounds are abundant in the atmosphere, it might be expected that the amount of SOA should depend importantly on temperature. However, laboratory results indicate that SOA nucleation and growth exhibit only a moderate T -dependence,^{58–60} with effective ΔH_{sub} values of 10–40 kJ/mol.^{59,61} Understanding the nature of the physical and chemical interactions that lead to this striking reduction in SOA sensitivity to temperature is of critical importance, although it is likely related to SOA being composed of multiple compounds which have a wide range of vapor pressures. Our results suggest that even relatively simple physical interactions (such as those between the diacids and alcohols or water) can dramatically influence the apparent thermodynamic properties of the system, suggesting interesting directions for future research.

When group-contribution methods are used to estimate vapor pressures of low-volatility compounds, we recommend the use of SPARC or Jensen-UNIFAC p_L^0 values, as both give reasonable agreement with our results, although caution must be exercised for larger N_c . Vapor pressures predicted by the Capouet and Müller or Asher-UNIFAC methods appear to greatly overestimate p_L^0 . We suggest that these temperature-dependent vapor pressure measurements can be used in the development of new, more accurate group-contribution parameter sets.

The majority of gas-particle partitioning models use pure component (subcooled liquid) vapor pressures with the assumption that the activity coefficient is unity, i.e., that the “solution” is ideal. However, the strong intermolecular interactions that cause these diacid molecules to have such low pure component vapor pressures will undoubtedly be changed in a many-component mixture, especially when hydrogen bonding is

important in the pure component. It has been stated that it is not unreasonable to assume that the activity coefficient is unity for individual components of a mixture composed of similar species.^{10,62,63} However, given the lack of definitive experimental evidence, we nonetheless urge caution when applying the pure component p^0 determined here to the modeling of gas-particle partitioning for real (i.e., multicomponent) aerosol systems.

Conclusions

We have developed a new temperature programmed desorption based method for direct determination of the evaporation rates of very low volatility compounds. Here, we have focused specifically on C_4 – C_{10} and C_{12} dicarboxylic acids. The method is similar to that of Chattopadhyay and Ziemann,²⁰ although it allows for direct measurements of evaporation rates as a function of temperature. The observed evaporation rates are used to estimate the vapor pressures of the diacids from the Hertz–Knudsen equation. The enthalpy and entropy of sublimation have also been measured. Our results suggest that the vapor pressures of the diacids are typically lower than those measured using TDMA^{16,17} or Knudsen cell^{13,14} or other TPD²⁰ methods. Despite this disparity in the absolute magnitude of $p^0(298\text{ K})$, the odd–even dependence previously observed for the diacids was confirmed. However, our measured ΔH_{sub}^0 and ΔS_{sub}^0 indicate that the odd–even dependence of $p^0(298\text{ K})$ results from only small deviations from linearity in these parameters with increasing carbon chain length, at least up to $N_c \leq 9$, as opposed to an exceedingly large odd–even dependence of these parameters themselves. Reasonable agreement between our experimental $p^0(298\text{ K})$ and that calculated from two group-contribution methods (SPARC²⁵ and UNIFAC using the Jensen et al. parameters²³) was found for the smaller N_c diacids, but our results differ from other calculations (Capouet and Müller⁴¹ and UNIFAC using the Asher et al. parameters²⁴).

Perhaps most importantly, the experimental results indicate the extreme importance of preheating of the samples. The influence of this preheating step appears to be 3-fold. First, it serves to drive off any extraneous sample that is subsequently observed as increased evaporation rates at lower temperatures. Second, preheating may lead to sintering of the samples, which may have changed the effective surface area. And, finally, preheating serves to drive any remaining solvent molecules (in this case, methanol) and other higher-volatility impurities out of the deposited sample. We postulate that this third effect is the primary reason for the discrepancy between these results and the previous TDMA and TPD measurements. In light of this, further measurements comparing the vapor pressures and ΔH_{sub}^0 values for other compounds, such as the homologous monocarboxylic acids, are clearly desirable.

Acknowledgment. We thank Troy Thornberry, Jim Burkholder, Joost de Gouw and Karl Froyd from NOAA, Paul Ziemann from UC Riverside and Merete Bilde from the University of Copenhagen for useful discussions.

Supporting Information Available: The Supporting Information contains a detailed description of the temperature-dependent sticking correction, additional figures related to the observed solvent effect and example temperature programmed desorption scans for each of the dicarboxylic acids considered in this study. This material is available free of charge via the Internet at <http://pubs.acs.org>.

References and Notes

- (1) IPCC *Climate Change 2001: The Scientific Basis. Contribution of Working Group I to the Third Assessment Report of the Intergovernmental Panel on Climate Change*; Cambridge University Press: Cambridge, U.K., 2001.
- (2) Pope, C. A.; Dockery, D. W.; Schwartz, J. *Inhal. Toxicol.* **1995**, *7*, 1.
- (3) Kanakidou, M.; Seinfeld, J. H.; Pandis, S. N.; Barnes, I.; Dentener, F. J.; Facchini, M. C.; Van Dingenen, R.; Ervens, B.; Nenes, A.; Nielsen, C. J.; Swietlicki, E.; Putaud, J. P.; Balkanski, Y.; Fuzzi, S.; Horth, J.; Moortgat, G. K.; Winterhalter, R.; Myhre, C. E. L.; Tsigaridis, K.; Vignati, E.; Stephanou, E. G.; Wilson, J. *Atmos. Chem. Phys.* **2005**, *5*, 1053.
- (4) de Gouw, J. A.; Middlebrook, A. M.; Warneke, C.; Goldan, P. D.; Kuster, W. C.; Roberts, J. M.; Fehsenfeld, F. C.; Worsnop, D. R.; Canagaratna, M. R.; Pszenny, A. A. P.; Keene, W. C.; Marchewka, M.; Bertman, S. B.; Bates, T. S. *J. Geophys. Res.-Atmos.* **2005**, *110*.
- (5) Heald, C. L.; Jacob, D. J.; Park, R. J.; Russell, L. M.; Huebert, B. J.; Seinfeld, J. H.; Liao, H.; Weber, R. J. *Geophys. Res. Lett.* **2005**, *32*, L18809.
- (6) Volkamer, R.; Jimenez, J. L.; San Martini, F.; Dzepina, K.; Zhang, Q.; Salcedo, D.; Molina, L. T.; Worsnop, D. R.; Molina, M. J. *Geophys. Res. Lett.* **2006**, *33*, L17811.
- (7) Tunved, P.; Hansson, H. C.; Kerminen, V. M.; Strom, J.; Dal Maso, M.; Lihavainen, H.; Viisanen, Y.; Aalto, P. P.; Komppula, M.; Kulmala, M. *Science* **2006**, *312*, 261.
- (8) Pankow, J. F. *Atmos. Environ.* **1987**, *21*, 2275.
- (9) Pankow, J. F. *Atmos. Environ.* **1994**, *28*, 185.
- (10) Pankow, J. F. *Atmos. Environ.* **1994**, *28*, 189.
- (11) Seinfeld, J. H.; Pandis, S. N. *Atmospheric Chemistry and Physics: From Air Pollution to Climate Change*; John Wiley: New York, 1998.
- (12) Kulmala, M. *Science* **2003**, *302*, 1000.
- (13) Davies, M.; Thomas, G. H. *Trans. Faraday Soc.* **1960**, *56*, 185.
- (14) da Silva, M. A. V. R.; Monte, M. J. S.; Ribeiro, J. R. *J. Chem. Thermodyn.* **1999**, *31*, 1093.
- (15) Rader, D. J.; McMurry, P. H. *J. Aerosol Sci.* **1986**, *17*, 771.
- (16) Tao, Y.; McMurry, P. H. *Environ. Sci. Tech.* **1989**, *23*, 1519.
- (17) Bilde, M.; Svenningsson, B.; Monster, J.; Rosenorn, T. *Environ. Sci. Technol.* **2003**, *37*, 1371.
- (18) Ray, A. K.; Davis, E. J.; Ravindran, P. J. *Chem. Phys.* **1979**, *71*, 582.
- (19) Chattopadhyay, S.; Tobias, H. J.; Ziemann, P. J. *Anal. Chem.* **2001**, *73*, 3797.
- (20) Chattopadhyay, S.; Ziemann, P. J. *Aerosol Sci. Technol.* **2005**, *39*, 1085.
- (21) Fredenslund, A.; Jones, R. L.; Prausnitz, J. M. *AIChE J.* **1975**, *21*, 1086.
- (22) Fredenslund, A.; Gmehling, J.; Rasmussen, P. *Vapor-Liquid Equilibria Using UNIFAC*; Elsevier: Amsterdam, 1977.
- (23) Jensen, T.; Fredenslund, A.; Rasmussen, P. *Ind. Eng. Chem. Fundam.* **1981**, *20*, 239.
- (24) Asher, W. E.; Pankow, J. F.; Erdakos, G. B.; Seinfeld, J. H. *Atmos. Environ.* **2002**, *36*, 1483.
- (25) Hilal, S. H.; Karickhoff, S. W.; Carreira, L. A. *QSAR Comb. Sci.* **2003**, *22*, 565.
- (26) Prausnitz, J. M.; Lichtenthaler, R. N.; Azevedo, E. G. *Molecular Thermodynamics of Fluid-Phase Equilibria*, 2nd ed.; Prentice Hall: Englewood Cliffs, NJ, 1985.
- (27) Kawamura, K.; Ikushima, K. *Environ. Sci. Technol.* **1993**, *27*, 2227.
- (28) Fraser, M. P.; Cass, G. R.; Simoneit, B. R. T. *Environ. Sci. Technol.* **2003**, *37*, 446.
- (29) Yue, Z. W.; Fraser, M. P. *Atmos. Environ.* **2004**, *38*, 3253.
- (30) Limbeck, A.; Kraxner, Y.; Puxbaum, H. *J. Aerosol Sci.* **2005**, *36*, 991.
- (31) Satsumabayashi, H.; Kurita, H.; Yokouchi, Y.; Ueda, H. *Atmos. Environ. Pt. A* **1990**, *24*, 1443.
- (32) Limbeck, A.; Puxbaum, H.; Otter, L.; Scholes, M. C. *Atmos. Environ.* **2001**, *35*, 1853.
- (33) Mochida, M.; Kitamori, Y.; Kawamura, K.; Nojiri, Y.; Suzuki, K. *J. Geophys. Res.-Atmos.* **2002**, *107*.
- (34) Kawamura, K.; Kasukabe, H.; Yasui, O.; Barrie, L. A. *Geophys. Res. Lett.* **1995**, *22*, 1253.
- (35) Kawamura, K.; Imai, Y.; Barrie, L. A. *Atmos. Environ.* **2005**, *39*, 599.
- (36) Hatakeyama, S.; Tanonaka, T.; Weng, J. H.; Bandow, H.; Takagi, H.; Akimoto, H. *Environ. Sci. Technol.* **1985**, *19*, 935.
- (37) Docherty, K. S.; Ziemann, P. J. *J. Chromatogr., Sect. A* **2001**, *921*, 265.
- (38) Docherty, K. S.; Kumboonlert, K.; Lee, I. J.; Ziemann, P. J. *J. Chromatogr., Sect. A* **2004**, *1029*, 205.
- (39) Gao, S.; Keywood, M.; Ng, N. L.; Surratt, J.; Varutbangkul, V.; Bahreini, R.; Flagan, R. C.; Seinfeld, J. H. *J. Phys. Chem. A* **2004**, *108*, 10147.
- (40) Gao, S.; Ng, N. L.; Keywood, M.; Varutbangkul, V.; Bahreini, R.; Nenes, A.; He, J. W.; Yoo, K. Y.; Beauchamp, J. L.; Hodyss, R. P.; Flagan, R. C.; Seinfeld, J. H. *Environ. Sci. Technol.* **2004**, *38*, 6582.
- (41) Capouet, M.; Müller, J. F. *Atmos. Chem. Phys.* **2006**, *6*, 1455.
- (42) de Gouw, J. A.; Howard, C. J.; Custer, T. G.; Baker, B. M.; Fall, R. *Environ. Sci. Technol.* **2000**, *34*, 2640.
- (43) Linstrom, P. J.; Mallard, W. G. NIST Chemistry WebBook, NIST Standard Reference Database Number 69; National Institute of Standards and Technology: Gaithersburg MD, 20899, June 2005 (<http://webbook.nist.gov>).
- (44) Smith, D.; Spänel, P. *Mass Spectrom. Rev.* **2005**, *24*, 661.
- (45) Spänel, P.; Smith, D. *Int. J. Mass Spectrom.* **1998**, *172*, 137.
- (46) Steinbacher, M.; Dommen, J.; Ammann, C.; Spirig, C.; Neftel, A.; Prevot, A. S. H. *Int. J. Mass Spectrom.* **2004**, *239*, 117.
- (47) Hertz, H. *Ann. Phys.* **1882**, *17*, 177.
- (48) Cammenga, H. K. *Evaporation Mechanisms of Liquids. In Current Topics in Materials Science*; Kaldis, E., Ed.; North-Holland Publishing Co.: Amsterdam, 1980; Vol. 5, pp 335.
- (49) Pound, G. M. *J. Phys. Chem. Ref. Data* **1972**, *1*, 135.
- (50) Kulmala, M.; Wagner, P. E. *J. Aerosol Sci.* **2001**, *32*, 833.
- (51) Fundamentally, the measured intercept is equal to $\Delta H_{\text{sub}}/RT^*$, not $\Delta S_{\text{sub}}/R$, where ΔH_{sub} is the determined value over the measurement range (T) and T^* is the temperature when $p^0 = 1$ atm, the reference state. However, $\Delta H_{\text{sub}}(T) = \Delta H_{\text{sub}}(T^*) + \Delta C_p(T - T^*)$, and therefore the intercept is $\Delta H_{\text{sub}}(T^*)/RT^* + (\Delta C_p/R)(T/T^* - 1)$, where ΔC_p is the standard molar heat capacity of sublimation. Because at equilibrium $\Delta H_{\text{sub}}/T = \Delta S_{\text{sub}}$, then the intercept is $\Delta S_{\text{sub}}(T)/R + \Delta C_p \ln(T^*/T) + (\Delta C_p/R)(T/T^* - 1)$, or simply $\Delta S_{\text{sub}}(T)/R$ assuming $C_p = 0$. For simplicity, we ignore the temperature conversion as this does not affect the general conclusions ($\Delta S_{\text{sub}}(T)$ values differ from the measured intercept by <4 J/(mol·K) assuming $\Delta C_p = -50$ J/(mol·K)) and allows for straightforward calculation of $p^0(T)$.
- (52) Hendricks, S. B. *Chem. Rev.* **1930**, *7*, 431.
- (53) Thalladi, V. R.; Nüsse, M.; Boese, R. *J. Am. Chem. Soc.* **2000**, *122*, 9227.
- (54) Cingolani, A.; Berchiesi, G. *J. Therm. Anal.* **1974**, *6*, 87.
- (55) Hilal, S. H.; Carreira, L. A.; Karickhoff, S. W. SPARC v 3.1, January 2006 (<http://ibmlc2.chem.uga.edu/sparc/>).
- (56) Atkins, P. W.; De Paula, J. *Physical chemistry*, 8th ed.; W. H. Freeman: New York, 2006.
- (57) Roux, M. V.; Temprado, M.; Chickos, J. S. *J. Chem. Thermodyn.* **2005**, *37*, 941.
- (58) Burkholder, J. B.; Baynard, T.; Ravishankara, A. R.; Lovejoy, E. R. Submitted to *J. Geophys. Res.*
- (59) Donahue, N. M.; Hartz, K. E. H.; Chuong, B.; Presto, A. A.; Stanier, C. O.; Rosenhorn, T.; Robinson, A. L.; Pandis, S. N. *Faraday Discuss.* **2005**, *130*, 295.
- (60) Pathak, R. K.; Stanier, C. O.; Donahue, N. M.; Pandis, S. N. *J. Geophys. Res.* **2007**, *112*, D03201.
- (61) Offenbergh, J. H.; Kleindienst, T. E.; Jaoui, M.; Lewandowski, M.; Edney, E. O. *Geophys. Res. Lett.* **2006**, *33*.
- (62) Jenkin, M. E. *Atmos. Chem. Phys.* **2004**, *4*, 1741.
- (63) Kamens, R.; Jang, M.; Chien, C. J.; Leach, K. *Environ. Sci. Technol.* **1999**, *33*, 1430.